Astron. Astrophys. 223, 47–60 (1989)

ASTRONOMY AND ASTROPHYSICS

H I rotation curves of spiral galaxies

I. NGC 3198

K. G. Begeman

Kapteyn Astronomical Institute, Groningen University, Postbus 800, NL-9700 AV Groningen, The Netherlands

Received December 14, 1988; accepted April 3, 1989

Summary. Observations of the spiral galaxy NGC 3198 in the 21 cm line using the Westerbork Synthesis Radio Telescope with an angular resolution of $25'' \times 35''$ are presented. The H I distribution extends to about two Holmberg radii and the radial velocity field is symmetric and regular over the entire area. A new method for the derivation of rotation curves is described. Results obtained show that the rotation curve of NGC 3198 is flat to within $5\,\mathrm{km\,s^{-1}}$ out to the last measured point at 11 disk scale lengths. This implies a large discrepancy between the observed rotation curve and that predicted from the light distribution.

Key words: galaxies: kinematics and dynamics of – galaxies: structures of – galaxies: NGC 3198

1. Introduction

Evidence for the existence of dark halos around spiral galaxies comes mainly from the flatness of rotation curves outside the visible region of galaxies with extended H I layers (e.g. Bosma, 1981). Since 21 cm line signals from these outer regions are weak, uncertainties in the rotational velocities at large radii for these older H I observations are relatively large. In addition, H I rotation curves in the inner regions are often imprecise because of poor angular resolution. As a result of these limitations only large-scale features of mass distributions derived from the early 21 cm line observations are meaningful.

Making use of improvements in the performance of the Westerbork Synthesis Radio Telescope in recent years, especially a decrease in system temperature leading to an increase in signal-to-noise ratio by a factor of two, several galaxies with extended H I envelopes were reobserved. The main aims of these observations are: (i) to measure the rotation curve with the highest possible precision, allowing a detailed comparison with the rotation curve predicted from the distribution of light, and (ii) to increase the extent of the region in which H I can be observed, possibly leading to a detection of an outer edge of the H I envelope.

Potential candidates for such a study must fulfil several criteria (see Sancisi and van Albada, 1987). The following galaxies were selected for reobservation: NGC 2841, NGC 3198, NGC 7331 (cf. Bosma, 1981) and NGC 5371 (cf. Wevers et al., 1986). In addition, existing data (Wevers et al., 1986) for NGC 2403, NGC 2903, NGC 5033 and NGC 6503 were reanalysed. The results from the main body of the author's Ph. D. thesis.

In the present paper I discuss the new observations of NGC 3198; the analysis of the mass distribution resulting from the rotation curve and the comparison with the light distribution have been published already (van Albada et al., 1985). Papers containing results for the other galaxies are in preparation.

2. Observations and data reduction

NGC 3198 is classified by de Vaucouleurs (1975) as a spiral of type SB(rs)c, the Holmberg (1958) dimensions are $11.'9 \times 4.'9$. In this paper we adopt a distance of 9.4 Mpc ($H_0 = 75\,\mathrm{km\,s^{-1}\,Mpc^{-1}}$). According to de Vaucouleurs (1975), NGC 3198 belongs to a loose group of galaxies (NGC 3184 group). Its nearest neighbour of comparable brightness (NGC 3184) lies at a projected distance of about 630 kpc. A blue photograph is shown in Fig. 1. The nucleus and the spiral arms are clearly visible but the inner ringlike structure, of dimensions $1.'7 \times 0.'5$, and the bar cannot be seen.

Bosma (1978, 1981) observed NGC 3198 with the WSRT 80-channel spectrometer. Neutral hydrogen was detected out to 1.5 Holmberg radii. The kinematics in the inner region (out to $1.'3$) has been studied by Cheriguène (1975) in Hα.

The observations described in this paper were obtained with the Digital Line Backend system at Westerbork (Bos et al., 1981). The WSRT observing parameters are summarized in Table 1. Compared to the observations done by Bosma (1981) we have about the same angular resolution but four times better sensitivity. After the standard Westerbork calibration procedures and Fourier transforms the data were processed further on the interactive reduction system (GIPSY) described by Allen et al. (1985). We obtained 63 channel maps with an angular resolution of $25'' \times 35''$ of which 25 maps contained line emission. The continuum emission was subtracted from the line channels by fitting a straight line through 26 continuum channels, 13 at the high frequency side of the galaxy and 13 at the low frequency side.

The sidelobes and grating rings in the 25 continuum free channel maps were removed with the standard CLEAN procedure (Högbom, 1974). The channel maps were restored by convolving the components found by the CLEAN algorithm with a Gaussian beam of the same HPBW as the original (dirty) beam. Because we did not have measurements at the short spacings, structures larger than $10'$ are strongly attenuated.

In an attempt to detect weak, extended H I emission the line channel maps were smoothed to a resolution of $70'' \times 70''$ and then cleaned. The increase in signal-to-noise ratio after the smoothing

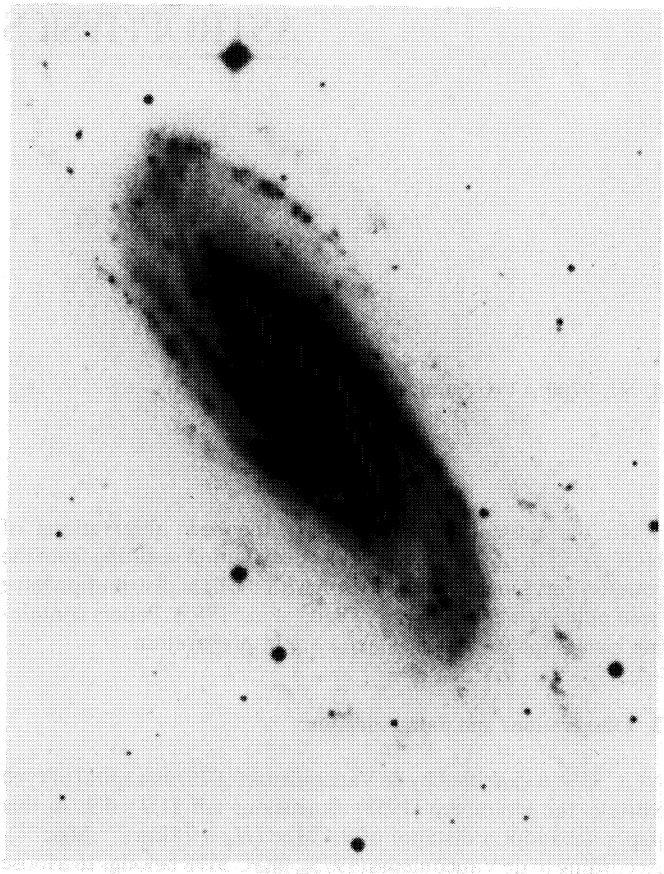

Fig. 1. Photograph of NGC 3198, kindly made available by J.W. Sulentic

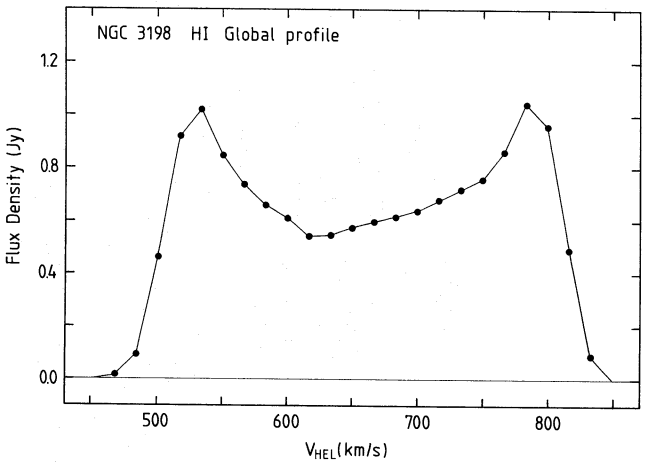

Fig. 2. Global H I line profile. The flux densities have been corrected for primary beam attenuation

Table 1. Westerbork observing parameters

Name of galaxy	NGC 3198
Dates of observation	25 and 26 April 1982
Length of observation	2×12^h
Number of interferometers	20
Baselines (min-max-increment)	36-1440-36 m
Synthesized beam	$25'' \times 35''$
Radii of first grating ring	$20'.2 \times 28'.2$
F.W.H.P. primary beam	$37'.5$
R.M.S. noise in channel maps	0.49 K
Central frequency	1417.3327 MHz
Velocity central channel (heliocentric)	650 km s^{-1}
Bandwidth	5.0 MHz
Number of channels	63
Channel separation	16.5 km s^{-1}
Velocity resolution	33.0 km s^{-1}
Field centre (1950.0)	$10^h16^m48^s$, 45°47′00″
K–mJy conversion, equivalent of 1 mJy/beam^{-1} area	0.71 K

was about a factor two. Except for a small extension of the southern part of the galaxy, no significant additional information was gained.

A global line profile (Fig. 2) was formed by adding together the fluxes of the individual components found by CLEAN and the residual fluxes for each channel map separately. The total amount of neutral hydrogen was derived by integrating this profile over all channels, yielding a H I mass of $(5.0 \pm 0.2)\ 10^9\ M_\odot$. Bosma found for the total H I mass a somewhat larger value of $5.5\ 10^9\ M_\odot$. Single dish measurements quoted in the literature show a large spread in the total H I mass (values ranging from $2.9\ 10^9\ M_\odot$ (Roberts, 1968) to $6.1\ 10^9\ M_\odot$ (Dickel and Rood, 1978)) and so cannot be used to determine the amount of neutral hydrogen lost in the WSRT observations due to the missing short spacings. Rots (1980) has mapped NGC 3198 in the 21 cm line with the 300 ft. Green Bank telescope and found a value of $4.7\ 10^9\ M_\odot$, which agrees well with the value found in this paper.

3. Results

3.1. *21 cm continuum*

An extended continuum source, with a small point source at the centre, is associated with NGC 3198. The instrumental responses of this continuum source and the background sources were removed with the CLEAN method. The continuum map (Fig. 3) is contaminated by an instrumental response caused by phase errors from a strong point source of 382 ± 17 mJy in the field at position (α, δ) $10^h16^m13^s.9$, 45°43′46″. The extent of the continuum emission of NGC 3198 is about $3'.5 \times 1'.5$ and the total flux density is 34 ± 4 mJy. There is no obvious correlation between the continuum emission and the optical spiral arms.

3.2. H I *distribution*

The cleaned channel maps containing line emission from the galaxy are shown in Fig. 3. It is clear from these channel maps that NGC 3198 behaves like a disk in differential rotation. The channel maps also show that NGC 3198 is fairly symmetric with respect to its centre. But there is some asymmetry with respect to the major axis, expecially in the northern part at radial velocities 551 and 584 km s^{-1}, where the emission at the eastern side extends farther out than on the western side.

A total hydrogen map was constructed by adding the cleaned channel maps. This was done for the full and the low resolution data. The total hydrogen map of the full resolution data is shown in Fig. 4. The dashed contour is the 3σ level of the low resolution hydrogen map.

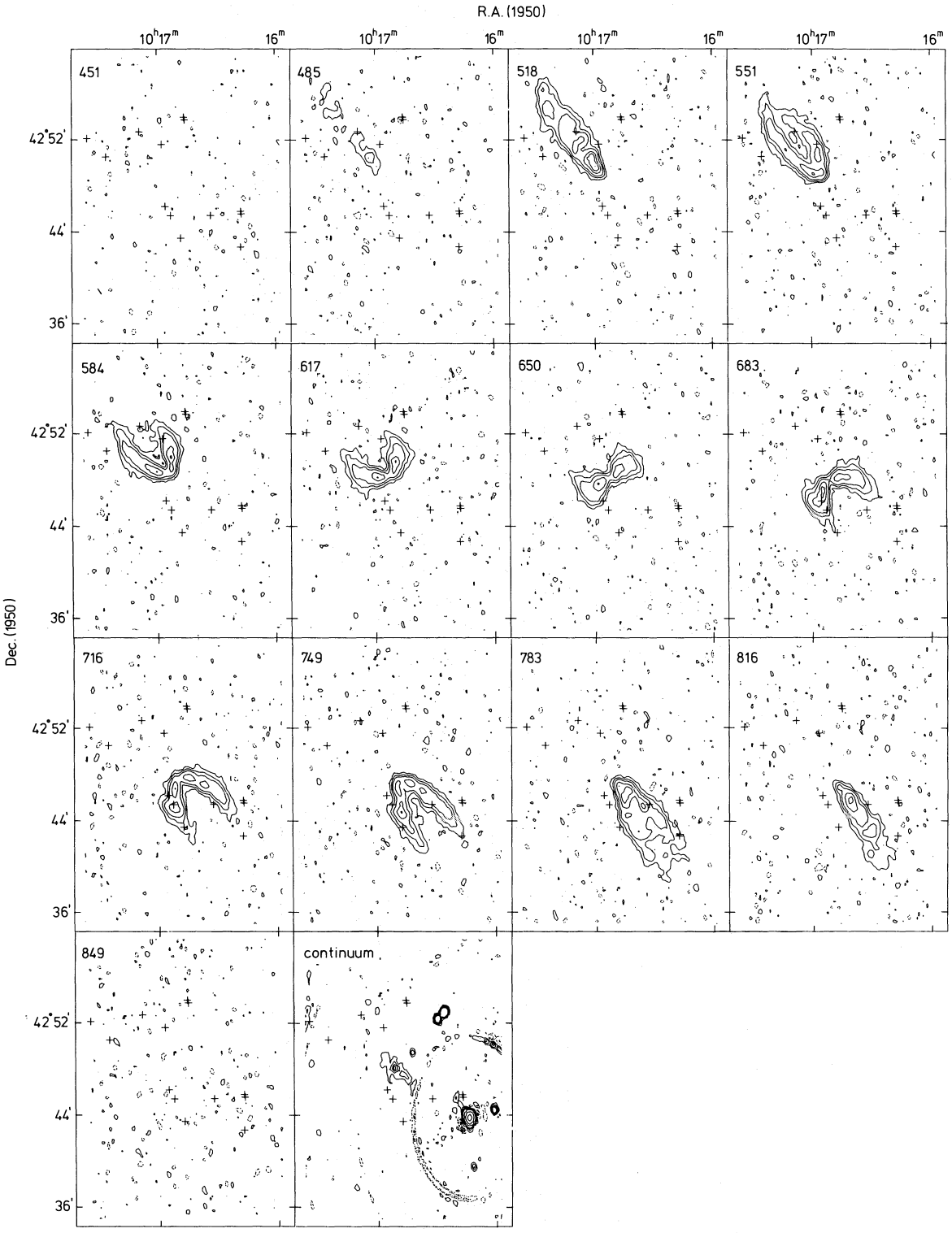

Fig. 3. Cleaned maps of the 21 cm line and continuum radiation. The size of the synthesized beam is 25″ × 35″. Contour levels are for the continuum map: −1, −0.5, 0.5, 1, 2, 8, 34, 135 K, and for the line maps: −1, 1, 3, 6, 13, 19, 26 K. Negative contours are shown dashed. The heliocentric velocity of each channel map is indicated in the upper left corner (km s^{-1}); the crosses refer to star positions. These maps have not been corrected for the primary beam attenuation

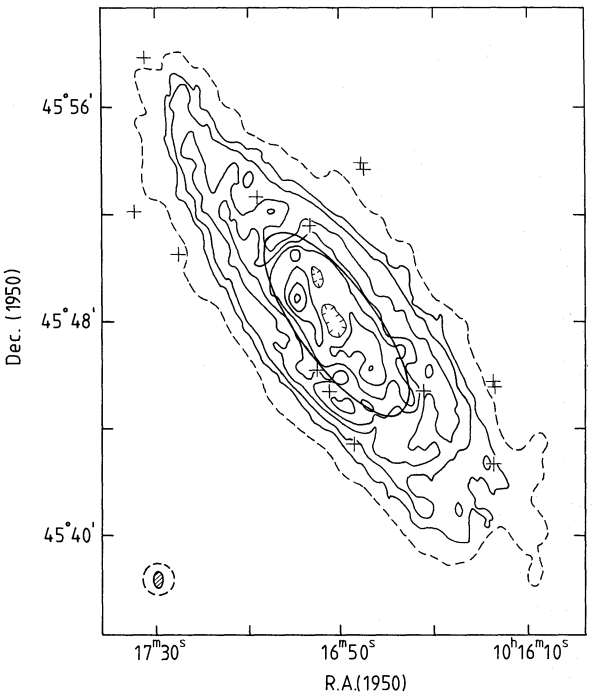

Fig. 4. Map of the H I column density distribution. The dashed contour is from low resolution data (70″ × 70″), the others from full resolution data (25″ × 35″). Contour levels are: 0.5 (3σ, low resolution), 1 (1σ, full resolution), 4, 8, 12, 16, 24, 28 10^{20} atom cm^{-2}. This map has been corrected for primary beam attenuation. The ellipse indicates the 25th mag arcsec^{-2} isophote (de Vaucouleurs et al., 1976). Tickmarks indicate local minima

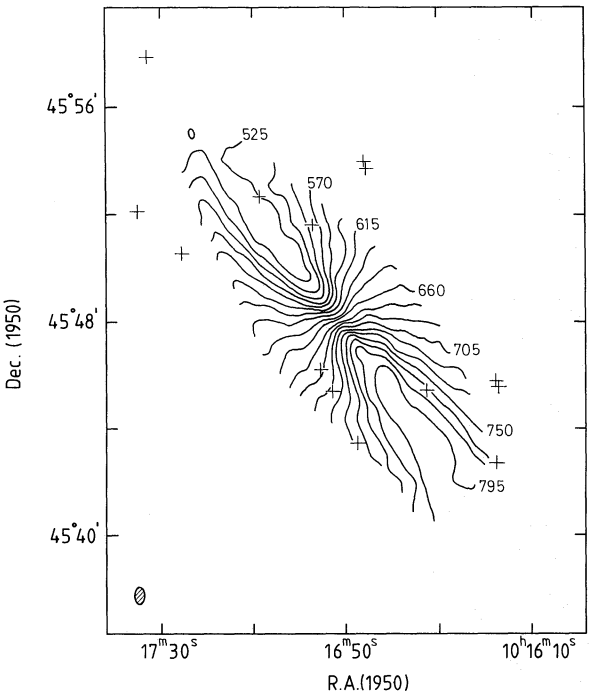

Fig. 5. Full resolution radial velocity field derived by fitting Gaussians to each line profile. The heliocentric radial velocities (km s^{-1}) are indicated

It is clear from Fig. 4 that the extent of the neutral hydrogen is much larger than the optical image of the galaxy. The H I distribution is not symmetric with respect to the centre, it is more extended in the northern half of the galaxy. However, the low resolution data show that weak neutral hydrogen emission is also present in the outer parts of the southern half. Near the centre there is a depression in the H I distribution, a feature common in spiral galaxies.

The optical spiral arms clearly correspond to enhancements in the neutral hydrogen distribution. In the northern part of the galaxy arm-like features are present with no visible optical counter part.

3.3. Velocity field

Because all the velocity profiles have a single peak and are quite symmetric (except in the inner region where beam-smearing causes some asymmetry), the fitting of single-peaked Gaussians to the profiles provides us with a good estimate of the mean radial velocity. The average width at half maximum of the profiles, corrected for instrumental effects, is about 32 km s^{-1}. As Fig. 5 shows, the resulting radial velocity field is very symmetric. There are some interesting features: (i) The velocity contours near the centre of the galaxy are twisted. In the north eastern and in the south western part the contours bend toward the kinematical major axis. This effect has also been noticed in models of barred galaxies, where the iso-velocity contours near the bar seem to be rotated towards the bar (Miller and Smith, 1979). The twist in the iso-velocity contours near the centre could thus indicate that there is a bar in NGC 3198 at a position angle somewhat larger than the position angle of the major axis. (ii) The position angle of the major axis varies somewhat with radius, especially in the southern part. (iii) In the north eastern part the iso-velocity contours show a sharp turn towards the south. Comparing the velocity field with the total H I map in Fig. 4 we find that this region coincides with an arm-like enhancement.

4. Determination of the rotation curve

To determine the rotation curve a tilted-ring model is fitted to the velocity field. We assume that the galaxy can be described by a set of concentric rings, each ring being characterised by a fixed value of the H I surface density and circular velocity V_C, and by two orientation angles (inclination angle i and position angle of major axis ϕ). Of these four parameters the H I surface density is taken directly from the observations but we solve for the other three through an iterative procedure. Each ring is also assigned a value for the systemic velocity (V_0), which is either constrained to be the same for all rings or kept as a free parameter. The values of the ring parameters are determined from the observed radial velocities in a set of concentric elliptic annuli in the plane of the sky, each one beamwidth (30″) wide along the major axis. Points on either side of the major axis are included up to an angle θ_{max}. Details of the iterative procedure used for finding the ring parameters are given in Appendix A.

A rather large number of points per annulus ($N = 30$) is needed for a meaningful solution of the unknown parameters. Therefore, the procedure is unreliable in the innermost regions of the galaxy. After each least-squares solution the distribution of the points (x, y) over the annuli may change somewhat due to changes in i and ϕ. This limits the convergence of the iteration process. But for $N > 30$ changes in the solution due to the changing membership of

points in the annuli are small with respect to the formal uncertainty of the solution. It may be noted that the solutions for V_C and i are coupled through the factor $V_C \sin(i)$ in Eq. (2). A closer inspection shows that the coupling of these two parameters depends strongly on i and θ_{max}. With θ_{max} at 45° the coupling is not very strong for inclinations ranging from 50° to 80°, and for inclinations around 70° the parameters are independent. Therefore an accurate kinematical inclination can be determined for each ring; typical uncertainties are about 1°, based on the total size of the error ellipse (see Appendix A).

This iterative scheme has certain advantages above the trial and error method used by Warner et al. (1973). First of all our algorithm is automatic, and second we get a fairly good idea of the uncertainty in the parameters V_0, V_C, i and ϕ from the least-squares fit.

The correction for beam-smearing described in Appendix B can easily be implemented in this algorithm. Starting with the initial estimates, we can calculate and apply the correction term for each data point before performing the least-squares fit. In the analyses of the velocity field of NGC 3198 discussed below, this correction is included.

4.1. *Systemic velocity*

First we use the algorithm to determine the systemic velocity of NGC 3198. This can be done by fitting all four parameters (V_0, V_C, i and ϕ) to the observed velocity field for each ring separately. The individual determinations of the systemic velocity (V_0) give consistent results: the largest difference from the average value is somewhat less than $2\,\mathrm{km\,s^{-1}}$. Consequently, for the systemic velocity of NGC 3198 we take the mean of the various – independent – ring solutions, $V_0 = 660.4 \pm 0.6\,\mathrm{km\,s^{-1}}$. For these solutions the position of the dynamical centre (x_0, y_0) was held fixed. To estimate the effect of an error in the position of the centre the process was repeated for a central position shifted by half a beam (15″) along the major axis, yielding a difference of $0.5\,\mathrm{km\,s^{-1}}$ compared to the former result. As a check we also determined the systemic velocity from the global H I profile by using the velocities at the 50% level. This resulted in a value of $659 \pm 3\,\mathrm{km\,s^{-1}}$ which is consistent with the value found from the least-squares fit. Taking the various sources of uncertainty into account we adopt for the systemic velocity of NGC 3198 $V_0 = 660.4 \pm 0.8\,\mathrm{km\,s^{-1}}$. For the derivation of the kinematical parameters discussed below V_0 is held fixed at this value. We believe that the uncertainty in V_0 due to instrumental errors, or errors connected with the observing procedure, is smaller than $1\,\mathrm{km\,s^{-1}}$.

4.2. *Symmetry of rotation curve*

The concept of rotation curve is applicable only if a galaxy shows large-scale axial symmetry. This can to some extent be tested by determining a rotation curve for the two halves separately. Results of this comparison are shown in Fig. 6. The similarity between the kinematical parameters of both halves is striking. The differences in rotational velocity are typically 3 to $5\,\mathrm{km\,s^{-1}}$, and the differences in inclination and in position angle are in the order of 1 to 2 degrees. These solutions are not sensitive to the adopted weighting as a function of azimuthal angle. To obtain the circular velocity beyond 9′.5 the solutions for $i(R)$ and $\phi(R)$ derived from the region inside 9′.5 were extrapolated to larger radii and only V_C was solved for. In this way we were able to derive rotational velocities out to 11′ for the northern and the southern half of the galaxy separately.

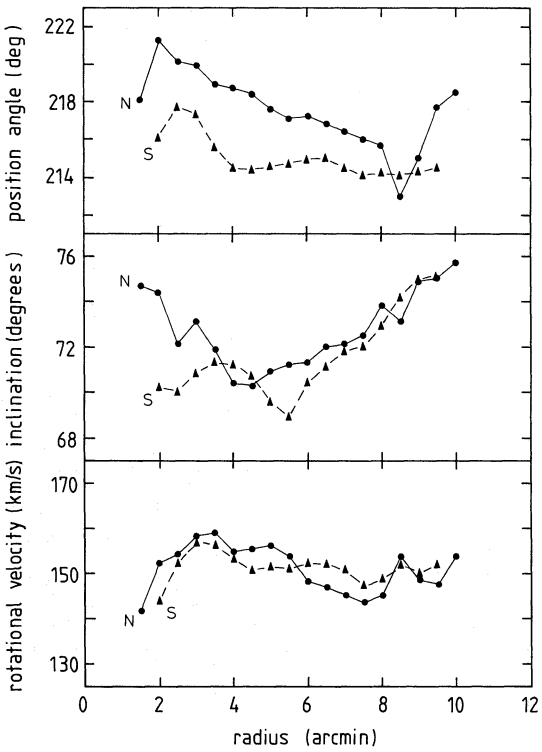

Fig. 6. The circular velocity, the inclination and the position angle as a function of radius as determined by the least-squares fitting algorithm for the northern half (dots) and the southern half (triangles) separately

4.3. *Inner regions*

The inner regions of NGC 3198 need a special treatment for two reasons: first, there are not enough data points available to make a complete least-squares fit and second, the velocity gradient in the inner parts of the velocity field causes significantly larger beam-smearing effects than in the outer regions. We therefore used the following method to determine the rotation velocities in the inner 4′. We assume that the position angle of the major axis and the inclination to the line of sight do not change with radius and we take for these parameters average values, i.e. $\phi = 216°$, $i = 71°.5$. Next we construct a position-velocity map along the major axis through the centre of the galaxy. At intervals of 15″ we take the velocity at the peak of each line profile to represent the radial velocity and divide by $\sin(i)$ to obtain a circular velocity uncorrected for beam-smearing. A rotation curve was derived by averaging the circular velocities of the northern and the southern half of the galaxy. This rotation curve is shown in Fig. 7a (line). For comparison, the least-squares method – with fixed inclination and position angle – was also applied to the inner regions with and without a correction for beam-smearing (see Appendix B). These results are also shown in Fig. 7a (crosses and dots). The agreement between the rotation curves derived from the position-velocity map and with the least-squares method without correction for beam-smearing is quite good. We are therefore led to adopt, provisionally, the least-squares solution *with* beam-smearing correction as the best estimate of the circular velocity.

The next question is: how far inward can we trust the correction for beam-smearing effects? In order to determine this, a model velocity field was calculated from an assumed rotation curve, shown in Fig. 7b (line). This velocity field was convolved with a Gaussian beam with the same HPBW as the synthesized

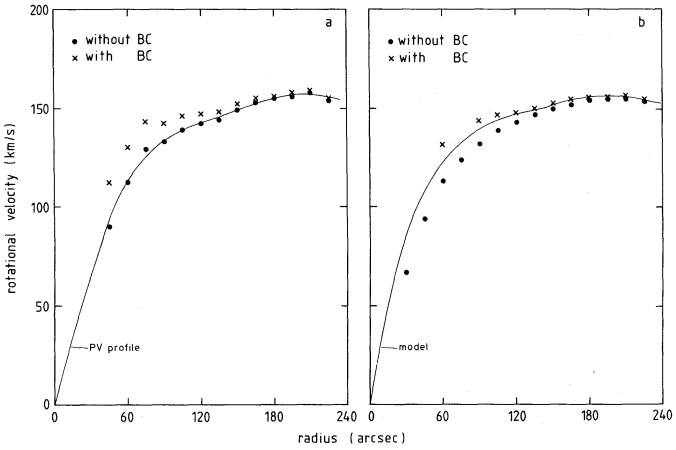

Fig. 7. **a** Rotation curve as derived from the position-velocity (PV) map along the major axis (line) together with the circular velocities resulting from the fit with (crosses) and without (dots) beam-smearing correction (BC). Note the excellent agreement between rotation curve from position-velocity map (line) and least-squares fit without beam-smearing corrections (dots). **b** Model rotation curve (line) together with the rotation curve derived from a least-squares fit with (crosses) and without (dots) beam-smearing correction. Note that the beam correction procedure works adequately for radii larger than 2′

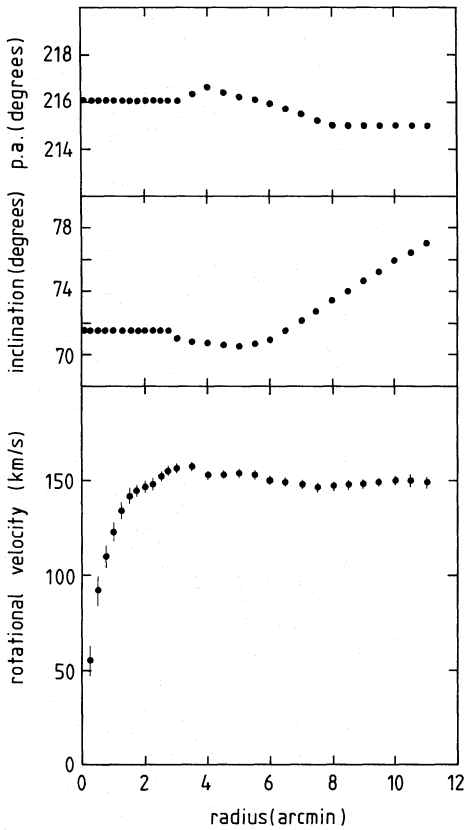

Fig. 8. Adopted circular velocity, inclination and position angle of NGC 3198

Westerbork beam (25″ × 35″). (For the H I distribution we took the observed distribution.) The least-squares algorithm with and without the correction for beam-smearing was used to determine a rotation curve from the convolved velocity field. The results are also shown in Fig. 7b (crosses and dots). We conclude from these model calculations that the least-squares method *with* the correction for beam-smearing gives satisfactory results (errors $< 1.5\,\mathrm{km\,s^{-1}}$) for radii larger than 1′.5. Inside 1′.5 the gradient in the rotation curve is large and this method does not produce a good estimate of the circular velocity. However, we can now obtain an estimate of the correction for beam-smearing by comparing the real (model) rotation curve with the rotation curve found by the algorithm *without* beam-smearing correction. In this way we get the following corrections to be applied to the rotation curve determined from the position-velocity map. Outside 1′.5, we added the difference between least-squares ring solution with and without beam-smearing corrections (Fig. 7a). Inside 1′.5, we added the difference between model rotation curve and rotation curve determined from convolved model velocity field (Fig. 7b). As an estimate of the errors in the circular velocities we take one third of the correction applied. We also checked the effect of the correction for beam-smearing for the outer regions (radii greater than 3′). The largest correction is about $4\,\mathrm{km\,s^{-1}}$. Outside 4′ no correction is needed ($< 1.5\,\mathrm{km\,s^{-1}}$).

In Fig. 8 we present the adopted kinematical parameters for NGC 3198 and in Table 2 we give the numerical values, which were obtained by averaging the parameters V_C, i and ϕ derived for the northern and southern half independently. The 1 σ errors were calculated from the difference between both halves. As a last check we used the least-squares algorithm on the whole galaxy, keeping i and ϕ fixed at the adopted values. The resulting rotation curve is consistent with the adopted one with differences $< 2\,\mathrm{km\,s^{-1}}$. In Fig. 9 we show the average rotation curve projected on a position-velocity map along the major axis.

Table 2. Rotation curve of NGC 3198

R (′)	V_C ($\mathrm{km\,s^{-1}}$)	ϕ (°)	i (°)	R (′)	V_C ($\mathrm{km\,s^{-1}}$)	ϕ (°)	i (°)
0.25	55±8	216.0	71.5	4.5	153±2	216.4	70.6
0.50	92±8	216.0	71.5	5.0	154±2	216.2	70.5
0.75	110±6	216.0	71.5	5.5	153±2	216.1	70.7
1.00	123±5	216.0	71.5	6.0	150±2	215.9	70.9
1.25	134±4	216.0	71.5	6.5	149±2	215.7	71.5
1.50	142±4	216.0	71.5	7.0	148±2	215.5	72.1
1.75	145±3	216.0	71.5	7.5	146±2	215.2	72.7
2.00	147±3	216.0	71.5	8.0	147±2	215.0	73.4
2.25	148±3	216.0	71.5	8.5	148±2	215.0	74.0
2.50	152±2	216.0	71.5	9.0	148±2	215.0	74.6
2.75	155±2	216.0	71.5	9.5	149±2	215.0	75.2
3.0	156±2	216.0	71.0	10.0	150±2	215.0	75.9
3.5	157±2	216.3	70.8	10.5	150±3	215.0	76.4
4.0	153±2	216.6	70.7	11.0	149±3	215.0	77.0

Notes: 1: This rotation curve has already been published by van Albada et al. 2: 1′ is 2.72 kpc at a distance of 9.4 Mpc. 3: The errors are derived from the difference between the kinematical parameters obtained for the northern and southern half separately, except for the circular velocities in the inner 90″, where 1/3 of the beam-smearing correction is taken.

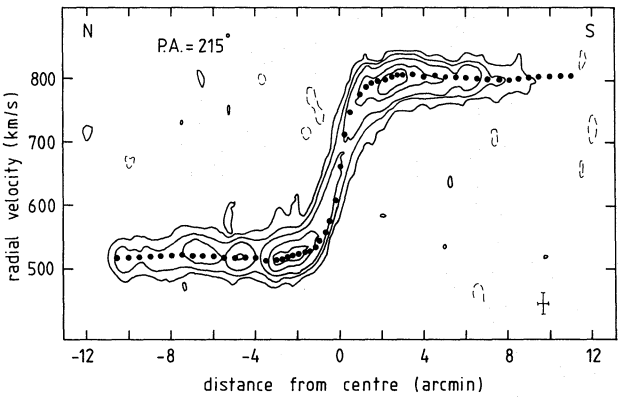

Fig. 9. The mean rotation curve for northern and southern half projected on a position-velocity map at a position angle of 215°. Contour levels are −1, 1, 3, 6, 13, 19 K. This map has not been corrected for primary beam attenuation

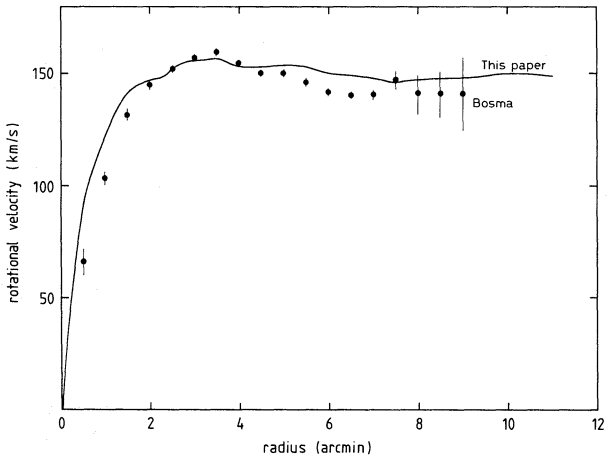

Fig. 10. Rotation curve derived by Bosma (dots) compared with the rotation curve derived in this paper (line)

5. Comparison of rotation curve with previous determinations

In Fig. 10 we show our final rotation curve, together with the rotation curve derived by Bosma (1981). Overall the two curves are very similar but there are some differences in detail. First consider the inner regions of NGC3198 (i.e. radii less than 2′), where the differences between both rotation curves are largest. We find that the rotation velocities derived in this paper are systematically larger (up to 26 km s^{-1} at a distance of 0′.5) than the values derived by Bosma. The discrepancy is due largely to the neglect of beam-smearing corrections by Bosma. Differences of a few km s^{-1} are caused by differences in the data sets and by the use of different methods to derive the rotation curve from the velocity field.

In the outer regions of NGC 3198 (i.e. at radii larger than 5′) our rotation curve is systematically higher than the rotation curve derived by Bosma; on average the difference is about 7 km s^{-1}, with a maximum difference of 10 km s^{-1}. This difference cannot be explained by the fact that Bosma adopts a constant inclination of 70°, while our least-squares algorithm indicates that the galaxy becomes more edge-on with increasing radius. If a constant inclination of 70° is used in the least-squares fit, we find an even larger circular velocity for the outer parts, increasing the difference between Bosma's rotation curve and ours (up to 12 km s^{-1}). In fact, a solution with constant inclination and position angle would give a rising rotation curve in the outer regions (see Wevers, 1984). Examining Bosma's residual velocities we get the impression that Bosma could have improved his fit with a somewhat larger rotation velocity in the outer regions (his model velocity field has an average residual with respect to the observed velocity field of about 10 km s^{-1}). It thus seems that Bosma, with his trial and error tilted-ring method, may not have found the optimum fit. In addition our signal-to-noise ratio is a factor 4 higher than Bosma's, which makes us feel confident about the rotation curve derived in this paper.

In Fig. 11 we show the radial velocities measured in Hα by Cheriguène (1975) along a position angle of 225° superimposed on a position-velocity plot of the H I along the same axis. The dashed curve indicates our rotation velocities (corrected for beam smearing) projected along the same axis. The agreement of our rotation curve with Cheriguène's data is not so good at 30″ (our circular velocity is about 20 km s^{-1} larger), but at 60″ and 90″ we are in complete agreement (Bosma made the same comparison and

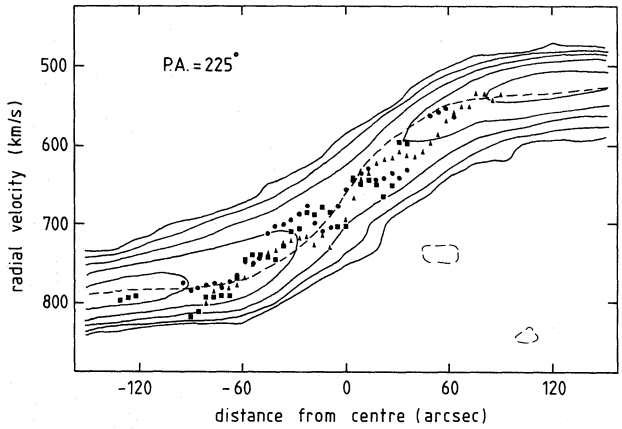

Fig. 11. Position-velocity map at position angle 225° superimposed on the radial velocities derived by Cheriguène. Different symbols indicate different measurements. The radial velocities predicted by our adopted rotation curve are shown by the dashed line

concluded from the agreement of his 21 cm line velocities and the optical data at 30″ that no correction for beam smearing was necessary). Recently, Hunter et al. (1986) obtained Hα rotation velocities of a higher quality for the inner 2′, and their rotation curve is in excellent agreement with our beam-corrected 21 cm rotation curve (maximum difference 3 km s^{-1}).

As a check of the assumption that the H I gas moves along circular orbits we have plotted the observed radial velocities corrected for beam-smearing minus the radial velocities predicted by our model against azimuthal angle. This plot is shown in Fig. 12 for a number of rings. On average the residual velocities are about 5 km s^{-1}, with the smallest deviation along the major axis. Note that only radial velocities ranging in θ from −45° to 45° were used in the least-squares fit, and that each data point was weighted with $|\cos(\theta)|$. There is a clear pattern in the differences between the model and observed velocity field. For radii ranging from 3′ to 6′ the residuals of the northern and southern half of NGC 3198 show the same trend: they both show a double periodic sinusoidal behaviour. The largest residual velocities appear at angles of about 40° and 220°; when projecting back to the plane of the sky

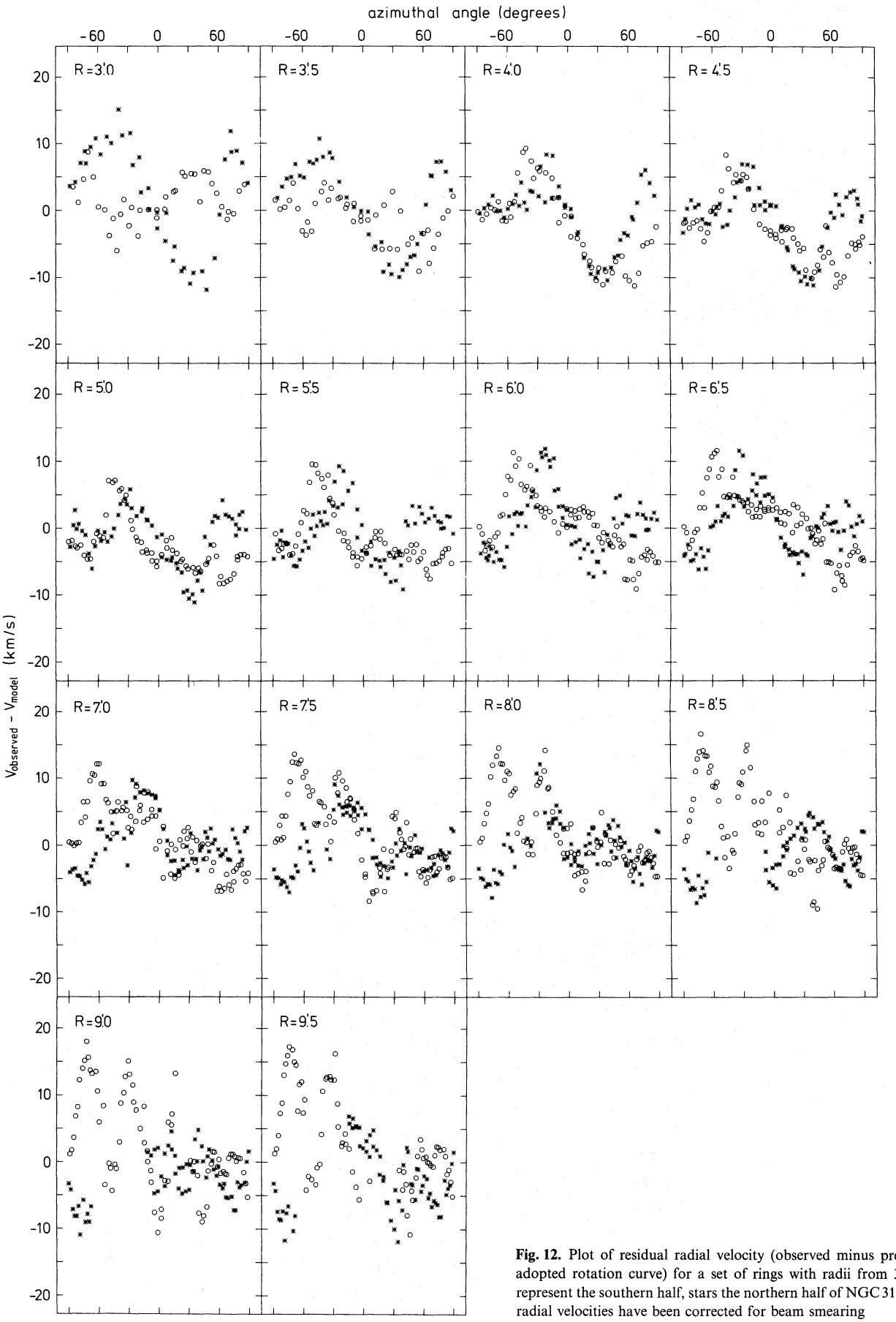

Fig. 12. Plot of residual radial velocity (observed minus predicted from the adopted rotation curve) for a set of rings with radii from 3′ to 9′.5. Circles represent the southern half, stars the northern half of NGC 3198. The observed radial velocities have been corrected for beam smearing

we find that these positions coincide with the optical spiral arms. Probably these double sinusoidal residual velocities are caused by streaming of the gas. (Note that with an incorrect choice of the inclination the velocity residuals would be symmetric with respect to the major axis, $\theta = 0°$, rather than antisymmetric as observed.)

6. The extent of the neutral hydrogen distribution

In Fig. 13 we have plotted the radial surface density profile of the neutral hydrogen for the northern half (dots) and the southern half (crosses) of NGC 3198 separately; the numerical values are given in Table 3. The surface densities were calculated by integration of the neutral hydrogen in rings with the parameters taken from the final fit. Overall the two curves are very similar, except in the outer regions, i.e. beyond 7′. Here the amount of neutral hydrogen in the southern half is decreasing rapidly to an almost constant value of $0.5\,M_\odot\,\mathrm{pc}^{-2}$, while in the northern half the amount of neutral hydrogen remains constant at a level of about $1.5\,M_\odot\,pc^{-2}$, and then at a radius of 9′ starts to decrease. This effect was investigated further by determining the surface density along the major axis of the galaxy. The advantage of doing this instead of integrating over all azimuthal angles is that now the distribution is not smoothed out in the azimuthal direction, and one can investigate the "edges" of NGC 3198 properly. We find that for the northern half the H I density falls off sharply from $(5.0\pm0.4)\ 10^{20}$ atom cm^{-2} at a radius of 10′.5 to $(0.5\pm0.4)\ 10^{20}$ atom cm^{-2} at a radius of 11′, while for the southern half the H I density falls off more gradually. Thus, apparently there is a sharp drop in the neutral hydrogen density in the northern half of NGC 3198 at a distance of 11′ from the centre. Using the low resolution (70″ × 70″) data, we find low level neutral hydrogen emission in the southern half. This is illustrated in Fig. 14, where we show a position-velocity map derived from the smoothed data (70″ × 70″) along a position angle of 218°. There is some low level emission in the southern half at a distance of 12′ from the centre. This gas is displaced from the major axis of the galaxy (Fig. 4), so it was not used for deriving the rotation curve. Its velocity and location are, however, consistent with circular motion and with the adopted rotation curve (linear extrapolation out to 13′).

We have also examined the velocity profile at the position of the strong continuum source (382 mJy; see Fig. 3) for the presence of absorption by the neutral hydrogen of NGC 3198. This point source lies at a projected distance of 7′.9 from the centre of NGC 3198 at position angle 237°, and is just outside the outer edge of NGC 3198 as observed in this paper. The distance from the

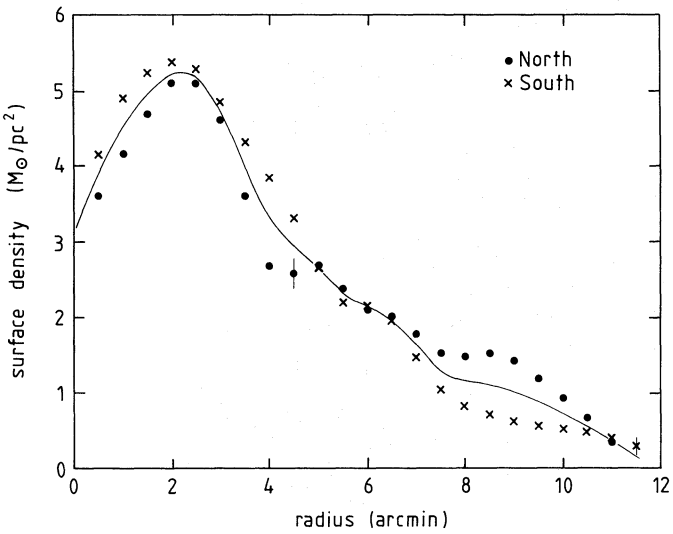

Fig. 13. Surface density of H I as a function of radius for the northern half (dots) and southern half (crosses) of NGC 3198. The line represents the average surface density

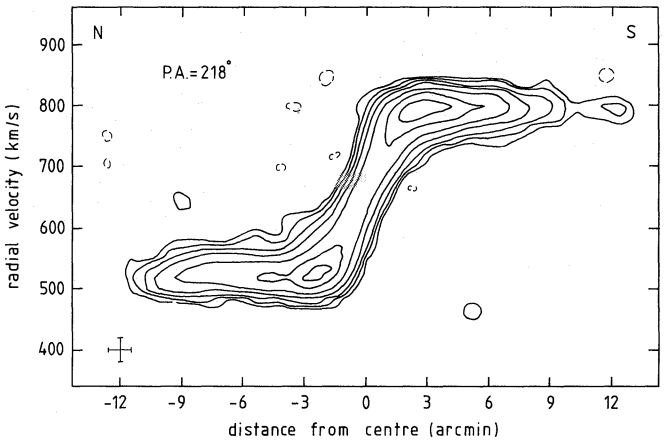

Fig. 14. Position-velocity map close to the major axis (position angle 218°, beam 70″ × 70″). The contour levels are: −0.3 (dashed), 0.3 (2σ), 0.6, 1.2, 2.4, 4.8, 9.6, and 14.4 K. This map has not been corrected for primary beam attenuation

Table 3. H I surface density of NGC 3198

R (′)	σ_{HI} ($M_\odot$ pc^{-2})	R (′)	σ_{HI} ($M_\odot$ pc^{-2})	R (′)	σ_{HI} ($M_\odot$ pc^{-2})	R (′)	σ_{HI} ($M_\odot$ pc^{-2})
0.0	3.17	3.0	4.73	6.0	2.12	9.0	1.01
0.5	3.88	3.5	3.95	6.5	1.98	9.5	0.86
1.0	4.53	4.0	3.26	7.0	1.62	10.0	0.72
1.5	4.97	4.5	2.94	7.5	1.27	10.5	0.57
2.0	5.24	5.0	2.66	8.0	1.14	11.0	0.36
2.5	5.19	5.5	2.29	8.5	1.11	11.5	0.14

Note: 1′ is 2.72 kpc at a distance of 9.4 Mpc

centre in the plane of the galaxy is about 15′, so any evidence of absorption would indicate a larger H I extent than observed in emission. Assuming the H I to be optically thin, we get the following relation for the column density:

$$N_{\rm H} = \frac{4.6\ 10^{18}\ T\sigma I_0}{I_{\rm C}}\ ({\rm atom\,cm^{-2}}), \qquad (1)$$

where T is the temperature of the neutral hydrogen (K), σ its velocity dispersion (km s^{-1}), I_0 the maximum absorption and $I_{\rm C}$ the continuum flux density (382 mJy). An examination of the velocity profile at the position of the continuum source does not show any indication of absorption, so we can only obtain an upper limit for the H I column density at 15′ from the centre. Taking $T = 100$ K, $\sigma = 10$ km s^{-1} and for I_0 3 times the noise level of the channel maps, we find: $N_{\rm H} < 0.3\ 10^{20}$ atom cm^{-2}, which is twice the noise level in the low resolution total hydrogen map.

7. Discussion

We have observed NGC 3198 in the 21 cm line, and have detected neutral hydrogen out to about 12′, which is twice the Holmberg radius of this galaxy. Further, we have derived a rotation curve out to 11′ by using a tilted-ring-model fitting technique. Some of the parameters of NGC 3198 determined in this study are listed in Table 4. The optical properties of NGC 3198 have been studied by Wevers (1984) who found that the light distribution has exponential shape with scale length about 1′. This means that we have measured rotational velocities out to 11 disk scale lengths, which is as far as we know the largest distance over which a rotation curve has yet been measured. This rotation curve does not show a decrease in circular velocity in the outer regions of the galaxy. Since the velocity field of NGC 3198 is regular and can be described well by tilted rings in circular rotation, this galaxy is an excellent case for studying the mass distribution. In Fig. 15 we have made a comparison of our measured rotation curve and the rotation curve predicted from the observable mass components, i.e. gas and stars. The contribution from the gas component was calculated from the averaged H I surface density (Fig. 13), corrected for the presence of helium (i.e. $\sigma_{\rm HI}$ multiplied by 1.4). The contribution from the luminous component was calculated from Kent's r-band data assuming a constant M/L ratio. For the total mass of the stellar disk we took 34 $10^9\ M_\odot$; giving the maximum allowed rotation velocity (see Fig. 15): this gives $M/L_B \simeq 3.8\ M_\odot/L_{B\odot}$ (L_B from de Vaucouleurs et al., 1976). It is clear that there is a large discrepancy between the observed

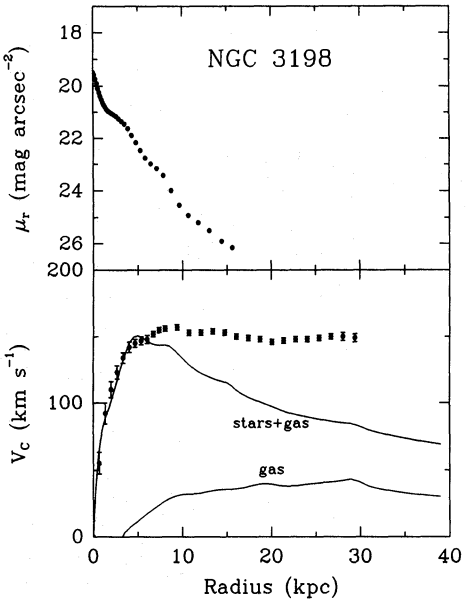

Fig. 15. Plot of observed rotation velocities (bottom) compared with rotation curve predicted from the photometric data (top, Kent, 1987) assuming a constant M/L ($3.8\ M_\odot/L_{B\odot}$) and z-thickness following a sech-squared law (van der Kruit and Searle, 1981) with disk thickness of 0.2 × the disk scale length. The contribution of the gas component has been included. The photometric data have not been corrected for inclination. Note the discrepancy between observed and predicted curves beyond 7 kpc

Table 4. Parameters of NGC 3198

Parameter	Value	Notes
Type	Sc(rs) I-II	1
Optical centre (1950.0)	$10^{\rm h}16^{\rm m}52\overset{\rm s}{.}1$ (±4″), 45°48′00″ (±3″)	2
Position 21 cm nucleus (1950.0)	$10^{\rm h}16^{\rm m}51\overset{\rm s}{.}3$ (±2″), 45°48′03″ (±3″)	3
V_0 heliocentric	660.4 ± 0.8 km s^{-1}	
Integrated H I-flux	242 ± 10 Jy km s^{-1}	
Distance	9.4 Mpc	4
$M_{\rm HI}$	(5.0 ± 0.2) $10^9\ M_\odot$	
L_B	(9.0 ± 0.9) $10^9\ L_{B\odot}$	5
L_V	(7.3 ± 0.7) $10^9\ L_{V\odot}$	5
Disk scale length	58″ (= 2.63 kpc)	6
R_{25}	4′.2	7
Holmberg diameter	11′.9 × 4′.9	8
21 cm continuum flux	34.0 ± 1.8 mJy	

Notes: 1: Sandage and Tammann (1981), 2: Gallouët et al. (1973). 3: Adopted dynamical centre. 4: $H_0 = 75$ km s^{-1} Mpc^{-1}. 5: Derived from de Vaucouleurs, de Vaucouleurs and Corwin (1976). 6: Wevers (1984). 7: Radius 25$^{\rm th}$ mag arcsec^{-2} isophote; de Vaucouleurs et al. (1976). 8: Holmberg (1958).

rotation curve and the one predicted from the luminous components. A further analysis of the mass distribution in NGC 3198 has been given by van Albada et al. (1985). The main conclusions from that paper are (i) the rotation curve of NGC 3198 can be described by a two-component mass model, consisting of an exponential disk and a spherical halo, and (ii) the amount of dark matter needed to explain the observed rotation curve out to the last measured point is at least a factor 4 larger than the amount of visible matter. A comparison of the mass distribution with that of other galaxies will be done in a future paper.

Appendix A. The tilted-ring model fit

The parameters which define the observed velocity field of a galaxy with a symmetrically rotating disk are the following:

1) The sky coordinates (x_0, y_0) of the rotation centre of the galaxy.

2) The velocity of the centre of the galaxy with respect to the sun, the so called systemic velocity V_0.

3) The circular velocity V_C at distance R from the centre.

4) The position angle ϕ of the major axis.

5) The angle i between the normal to the plane of the galaxy and the line-of-sight, the inclination angle.

The position angle of the major axis ϕ is defined here as the angle taken in anti-clockwise direction between the north direction on the sky and the major axis of the receding half of the galaxy (see e.g. Rots, 1975). Since the orientation angles i and ϕ and the rotation velocity V_C are expected to be a function of radius R, we will assume that the galaxy can be described by a set of concentric rings, each ring being characterized by a fixed value of i, ϕ and V_C. For a given ring the observed radial velocities recorded on a set of sky-coordinates (x, y) are related to the basic parameters by:

$$V(x, y) = V_0 + V_C(R) \sin(i) \cos(\theta). \quad (2)$$

In this expression θ is the azimuthal angle in the plane of the galaxy, related to the parameters i, ϕ, x_0 and y_0 through:

$$\cos(\theta) = \frac{-(x-x_0)\sin(\phi) + (y-y_0)\cos(\phi)}{R}, \quad (3a)$$

$$\sin(\theta) = \frac{-(x-x_0)\cos(\phi) - (y-y_0)\sin(\phi)}{R\cos(i)}, \quad (3b)$$

where R is the mean radius of the ring in the plane of the galaxy.

From Eq. (2) it is clear that the determination of the orientation parameters from the observed velocity field is not straightforward, because each set of parameters i, ϕ, x_0, y_0 defines a different set of sky coordinates x, y. Therefore we propose the following iterative procedure to determine the basic parameters:

1) Divide the galaxy into concentric rings with typical widths of one beam on the major axis.

2) Estimate initial values for the parameters V_0, x_0, y_0, V_C, i and ϕ. The position of the centre x_0, y_0 and the orientation angles i and ϕ can usually be taken from optical data or from the orientation of the neutral hydrogen disk of the galaxy (determined with e.g. ellipse fits).

3) From these estimates, calculate initial values of the radial velocities for the set of sky coordinates x, y defined by the parameters i, ϕ, x_0, y_0.

4) Make a least-squares fit for the parameters V_0, x_0, y_0, V_C, i and ϕ, using the observed velocity field $V_{obs}(x, y)$ and the initial guess determined above. Different weights can be assigned to the radial velocities in each annulus. The choice of the weighting function will be discussed later.

5) The improved values for the basic parameters define a new set of sky coordinates x, y. Steps 3) and 4) are repeated until a certain level of convergence has been reached. The iteration process is monitored by calculating χ^2.

This iterative procedure has certain advantages over the trial and error method used by Warner et al. (1973). First, the present algorithm is automatic, except for the choice of the initial parameters. Second, the method provides a fairly good estimate of the uncertainty in the parameters, and third the coupling between the basic parameters, e.g. V_C and i, is taken care of automatically by the least-squares routine. This coupling will be investigated in more detail in Sect. A2.

The least-squares method used by van Moorsel and Wells (1985) has the same advantages as the algorithm advocated here, but it does not allow a tilted-ring model. In other words, their method cannot account for changes in inclination and position angle of the major axis.

A1. Using the algorithm

When the tilted-ring model fit is applied to the observed velocity field of a galaxy, it will determine the parameters V_0, x_0, y_0, V_C, i and ϕ for each ring independently. The parameters V_0, x_0 and y_0 are special in this respect, since they should be the same for each ring. As a matter of fact, Eqs. (2) and (3) show that these parameters depend only on the symmetry of the velocity field (with respect to the centre). Therefore one can first use the algorithm to determine the systemic velocity and the position of the centre by keeping the other parameters fixed in the least-squares fit at their initial estimates, and solve for V_0, x_0, and y_0 only. When the results do not show systematic effects, i.e. when the observed velocity field is indeed symmetric, the best estimates for V_0, x_0, and y_0 are obtained by taking the mean over all rings. An estimate of the uncertainty in these mean values (1σ errors) is obtained by dividing the standard deviation from the mean by the square-root of the number of rings. After having determined the parameters V_0, x_0, and y_0, the algorithm can be used to solve for the parameters which are changing with radius, with the systemic velocity and the position of the centre kept fixed at their mean values.

This use of the algorithm has the advantage that one can now determine the parameters V_C, i and ϕ for the receding and approaching half of the galaxy separately, which provides a check on the symmetry of the velocity field. Obviously, it is not possible to determine the systemic velocity and position of the centre from one half of the galaxy only.

In a similar way one could try to fit the position angle of the major axis only (keeping V_0, x_0 and y_0 fixed), since this parameter is determined by the symmetry of the velocity field with respect to the major axis.

A problem still to be investigated is which weights to apply to the radial velocities in the least-squares fit. In principle there is no objection to the use of equal weights, except when the uncertainties in the determination of the radial velocities are known to be different. (In general these uncertainties are *not* known.) The following considerations, however, make the use of non-uniform weights preferable. Consider for example a galaxy with inclination and position angle of the major axis varying with radius, i.e. a warped disk. Then different annuli will overlap at certain sky positions. This means that at these positions one cannot uniquely define the annulus to which the observed radial velocities belong.

Since these effects are not present close to the major axis (for galaxies with moderate warps), one should give higher weight to radial velocities at positions close to the major axis. Furthermore, radial velocities at positions close to the minor axis carry less information about the underlaying circular velocity than at positions close to the major axis. Also for this reason one should give more weight to positions close to the major axis. A typically weighting function which would do this is $|\cos(\theta)|$. One could go even further and exclude all radial velocities at positions beyond a certain azimuthal distance from the major axis (θ_{max}). A typical value for θ_{max} for galaxies with moderate warps used in this thesis is 45°, but θ_{max} should be decreased when the warping of the disk gets stronger. Note however that information at points away from the major axis is needed to determine the inclination.

Another problem one must consider using the algorithm is the correlation between radial velocities recorded on adjacent coordinates, i.e. positions with separations less than the beam size of the telescope. Because the number of sampling points is larger than the number of independent beams this will result in an underestimate of the formal errors in the parameters. In general data are recorded at sampling intervals of about two points per resolution element, i.e. four points per beam. If only independent points would have been used, the formal errors in the parameters would be a factor of two larger. This factor of two is probably an upper limit to the correction required. One should use this upper limit to be on the safe side, since the real correlation among data points is difficult to obtain.

A2. The correlation between V_C and i

In Eq. (2) the rotational velocity V_C and the inclination i enter in the form of their product $V_C \sin(i)$, which is constant for each annulus. This could indicate that it is not possible to derive these two parameters separately. Clearly, the separation of V_C and i depends on the inclination dependence of θ.

In order to test whether it is possible to discriminate between different values for V_C and i, but with $V_C \sin(i)$ kept constant, three model velocity fields were constructed, each having a constant radial velocity beyond a certain radius along the major axis; the first model with a declining rotation curve and increasing inclination, the second with a rising rotation curve and decreasing inclination, and the third with a flat rotation curve and constant inclination. To make these models realistic, random uncorrelated Gaussian noise with a mean error of 5 km s^{-1} was added.

The tilted-ring model fit was applied to these velocity fields to solve for the rotational velocity and inclination only. A $|\cos(\theta)|$ weighting function for the radial velocities was used with $\theta_{max} = 45°$. The initial estimates used for V_C and i were identical for the three cases and constant with radius. The solutions found for each ring are shown in Fig. 16 (dots), together with the exact values (lines). From Fig. 16 we may conclude that the agreement between the least-squares results and the input model is excellent. Furthermore we see that although the r.m.s. errors in the radial velocities for all three models were the same, the (1σ) errors in the fitted parameters are different. The errors for model 1, with inclination increasing with radius, are larger by almost a factor two. This can be explained by the fact that for this particular model the inclination angle changes in such a way that the different annuli will overlap. Another feature worth pointing out is that the errors in the fitted parameters decrease with radius. This can simply be explained by the fact that the number of points per annulus increases with radius.

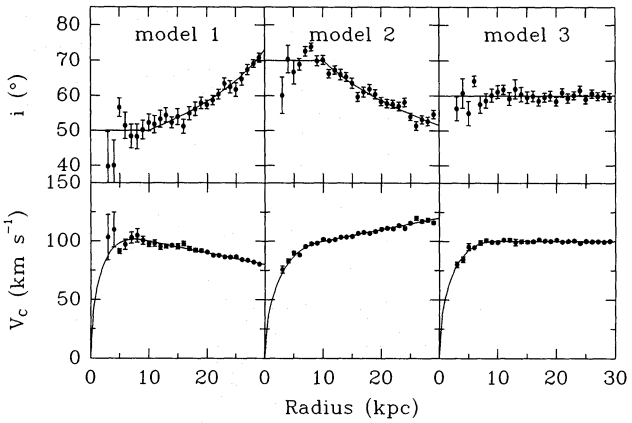

Fig. 16. The tilted-ring model fit for three model velocity fields. Lines denote the input parameters V_C and i for the models, the dots with error bars represent the results from the least-squares fitting algorithm

Let us now investigate how the rotational velocity and the inclination are coupled. In order to investigate the coupling, we study the χ^2 values of the fits as a function of V_C and i. For this purpose eight model velocity fields were constructed with inclinations ranging from 10° to 80°, and V_C constant at 100 km s^{-1}. Uncorrelated Gaussian noise was added with $\sigma = 3$ km s^{-1}. For each velocity field χ^2 was calculated as a function of V_C and i for one annulus only. This was done using a $|\cos(\theta)|$ weighting function and different values of θ_{max}. The resulting values of χ^2 were converted into probabilities. In Fig. 17 we show these probabilities as a function of V_C and i for different values of the inclination of the system and the cut-off value for θ. The contour levels are comparable to the 1, 2, 3, 4, and 5σ error levels for the parameters V_C and i. Figure 17 shows that the expected correlation of V_C and i is clearly present for inclination angles less than 60°. No change in this correlation with varying values of θ_{max} is present for these inclinations. For inclination angles greater than 60° the orientation of the error ellipses changes. At $i = 80°$ the correlation is even in the opposite direction. Note that for $i \simeq 70°$ there is hardly any correlation between V_C and i. It should be pointed out that the least-squares routine takes care of the correlation among parameters in the formal errors by projecting the major axis of the error ellipse on the parameter axes.

This exercise further shows that it is not possible to determine kinematical inclinations for galaxies which are close to face-on, i.e. inclination angles less than 40°. Moreover, one should keep in mind that the accuracy of the radial velocity field is also of importance; more precise determination of the radial velocities will lead to more accurate rotation curves. This means that for galaxies close to face-on the radial velocity field needs to be very accurately determined to obtain rotation curves with a reasonable precision (errors less than 1 km s^{-1} are required).

Appendix B. The effect of beam-smoothing

Consider the following simplification: let $N(x, y)$ denote the projected neutral hydrogen distribution of a galaxy in the plane of the sky, and let $V(x, y)$ be the velocity field of the galaxy, at rectangular coordinates x and y. Now assume that the velocity profiles at each position of the sky have a Gaussian shape with dispersion $S(x, y)$ and amplitude $N(x, y)/(\sqrt{2\pi}\, S(x, y))$. Let

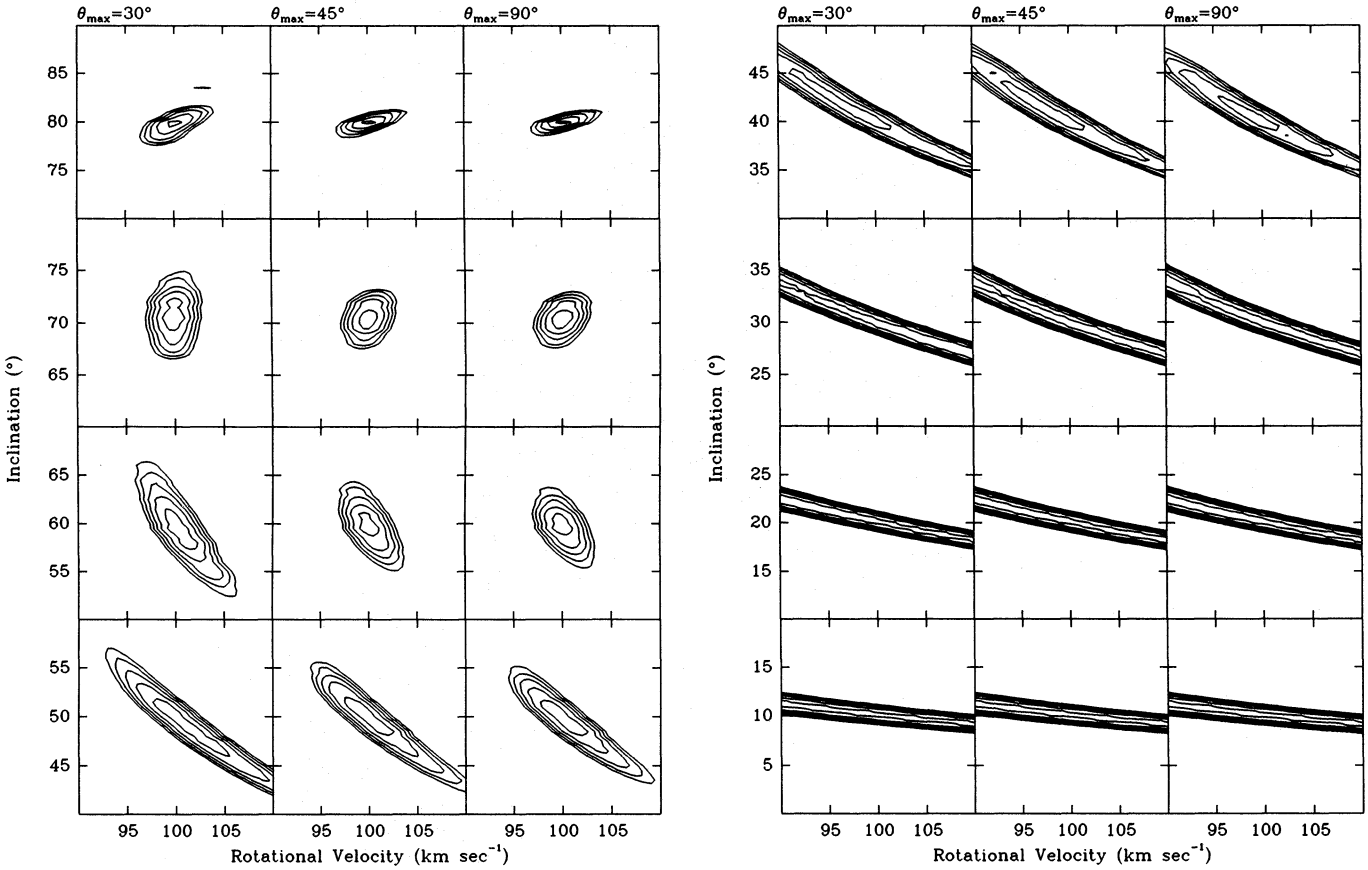

Fig. 17. χ^2 as a function of V_C and i for different values of θ_{max}. Contour levels correspond with the 1, 2, 3, 4, and 5σ probability levels

$n(x, y; v)$ denote the amount of neutral hydrogen at position (x, y) and at velocity v observed with a Gaussian beam

$$B(x,y) = 2\pi\alpha\beta \exp\left(-\frac{x^2}{2\alpha^2} - \frac{y^2}{2\beta^2}\right). \tag{4}$$

Then it follows that:

$$n(x,y;v) = \int_{-\infty}^{+\infty}\int_{-\infty}^{+\infty} d\xi\, d\eta \frac{N(\xi,\eta)}{\sqrt{2\pi}\,S(\xi,\eta)} \cdot \exp\left(-\frac{(v-V(\xi,\eta)^2)}{2S^2(\xi,\eta)}\right) B(x-\xi, y-\eta). \tag{5}$$

Calculating the observed moments $m_n(x,y) = \int_{-\infty}^{+\infty} dv\, v^n N(x,y;v)$ we find:

$$m_0(x,y) = \int_{-\infty}^{+\infty}\int_{-\infty}^{+\infty} d\xi\, d\eta\, N(\xi,\eta)\, B(x-\xi, y-\eta) = n(x,y) \tag{6}$$

and

$$m_1(x,y) = \int_{-\infty}^{+\infty}\int_{-\infty}^{+\infty} d\xi\, d\eta\, N(\xi,\eta)\, V(\xi,\eta)\, B(x-\xi, y-\eta). \tag{7}$$

Defining $w(x,y)$ as the observed intensity-weighted-mean velocity field, we find that: $w(x,y) = m_1(x,y)/m_0(x,y)$. To evaluate the integral expressions for $m_0(x,y)$ and $m_1(x,y)$ we expand $N(x,y)$ and $V(x,y)$ in a Taylor series around x and y, and neglect products of second derivatives. We then find:

$$w(x,y) = V(x,y) + \frac{1}{n(x,y)}\left(\frac{\partial V}{\partial x}\frac{\partial N}{\partial x}\alpha^2 + \frac{\partial V}{\partial y}\frac{\partial N}{\partial y}\beta^2\right) + \frac{N(x,y)}{2n(x,y)}\left(\frac{\partial^2 V}{\partial x^2}\alpha^2 + \frac{\partial^2 V}{\partial y^2}\beta^2\right). \tag{8}$$

We have now derived a simple relation between the true $(V(x,y))$ and the observed $(w(x,y))$ radial velocity field. The correction term represents the effect of beam-smearing described in Sect. 4. It still contains the unknown true HI distribution and the true velocity field. In order to estimate the correction, we take for $N(x,y)$ the observed distribution, and use for $V(x,y)$ a model velocity field.

Acknowledgements. The author wishes to thank T.S. van Albada and R. Sancisi for helpful comments and discussions and S. Casertano for his help with the software for calculating model rotation curves. This work was partly supported by the Netherlands Foundation for Astronomical Research (ASTRON) with financial support from the Netherlands Organization for the Advancement of Pure Research (ZWO).

The Westerbork Synthesis Radio Telescope is operated by the Netherlands Foundation for Radio Astronomy which is financially supported by the Netherlands Organization for the Advancement of Pure Research (ZWO).

References

van Albada, T.S., Bahcall, J.N., Begeman, K., Sancisi, R.: 1985, *Astrophys. J.* **295**, 305

Allen, R.J., Ekers, R.D., Terlouw, J.P.: 1985, *Proc. Intern. Workshop on Data Analysis in Astronomy at Erice*, eds. L. Scarci, V. di Gesu, Plenum, London

Begeman, K.: 1987, Ph.D. thesis, Groningen University, Chapter 3

Bos, A., Raimond, E., van Someren Greve, H.W.: 1981, *Astron. Astrophys.* **98**, 251

Bosma, A.: 1978, Ph.D. thesis, Groningen University

Bosma, A.: 1981, *Astron. J.* **86**, 1791

Cheriguène, M.F.: 1975, *La Dynamique des Galaxies Spirale*, Colloques Internationaux du C.N.R.S. **241**, 439

Dickel, J.R., Rood, H.J.: 1978, *Astrophys. J.* **223**, 391

Gallouët, L., Heidmann, N., Dampierre, F.: 1973, *Astron. Astrophys. Suppl. Ser.* **12**, 89

Högbom, J.A.: 1974, *Astron. Astrophys. Suppl. Ser.* **15**, 417

Holmberg, E.: 1958, *Medd. Lund Obs. Ser.* II, No. 136

Hunter, D.A., Rubin, V.C., Gallagher, J.S.: 1986, *Astrophys. J.* **91**, 1086

Kent, S.: 1987, *Astron. J.* **93**, 816

van der Kruit, P.C., Searle, L.: 1981, *Astron. Astrophys.* **95**, 105

Miller, R.H., Smith, B.F.: 1979, *Astrophys. J.* **227**, 785

van Moorsel, G.A., Wells, D.C.: 1985, *Astron. J.* **90**, 1038

Roberts, M.S.: 1968, *Astron. J.* **73**, 417

Rots, A.H.: 1975, *Astron. Astrophys.* **45**, 43

Rots, A.H.: 1980, *Astron. Astrophys. Suppl. Ser.* **41**, 189

Sancisi, R., van Albada, T.S.: 1987, in *Dark Matter in the Universe*, *IAU Symp.* **117**, eds. J. Kormendy, G.R. Knapp, Reidel, Dordrecht

Sandage, A., Tammann, G.A.: 1981, *Revised Shapley-Ames Catalogue of Bright Galaxies*, Carnegie Inst. of Washington Publ., No. 635

de Vaucouleurs, G.: 1975, *Stars and Stellar Systems* **9**, 557

de Vaucouleurs, G., de Vaucouleurs, A., Corwin, H.G.: 1976, *Second Reference Catalogue of Bright Galaxies*, University of Texas Press, Austin

Warner, P.J., Wright, M.C.M., Baldwin, J.E.: 1973, *Monthly Notices Roy. Astron. Soc.* **163**, 163

Wevers, B.M.H.R.: 1984, Ph.D. thesis, Groningen University

Wevers, B.M.H.R., van der Kruit, P.C., Allen, R.J.: 1986, *Astron. Astrophys. Suppl. Ser.* **66**, 505